ISSN 0304-9892 (Print) ISSN 2455-7463 (Online)
www.vijnanaparishadofindia.org/jnanabha
***Jñānābha*, Vol. 53(1) (2023), 263-271**
(Dedicated to Professor G. C. Sharma on His 85^{th} Birth Anniversary Celebrations)

IMPACT OF MELTING ON MHD HEAT AND MASS TRANSFER OF CASSON FLUID FLOW OVER A STRETCHING SHEET IN POROUS MEDIA IN PRESENCE OF THERMAL RADIATION AND VISCOUS DISSIPATION

Hina Yadav and Mamta Goyal
Department of Mathematics, University of Rajasthan, Jaipur, India-302004
Email: hinarao297@gmail.com, mamtagoyal1245@gmail.com

(Received: April 20, 2022; In format: May 12, 2022; Revised: May 26, 2023; Accepted: June 15, 2023)

DOI: https://doi.org/10.58250/jnanabha.2023.53131

Abstract

Impact of melting on MHD heat and mass transfer of Casson fluid flow over a stretching sheet in porous media with thermal radiation and viscous dissipation have been investigated in this article. Governing PDE's are change into coupled ODE 's using a set of proper similarity transformation. Resultant equations are solved by efficient numerical scheme Runge kutta- 4^{th} order allied with shooting method. Impact of several flow parameters on flow fields are interpreted via tables and graphs. Present outcomes compared with existing results and observed excellent validation.

2020 Mathematical Sciences Classification. 76W05, 76D05 ,76Sxx, 80A19, 78A40.

Keywords and phrases. MHD, Casson fluid, Porous medium, Heat and mass transfer, Radiation, Viscous dissipation..

1 Introduction

Investigation of non-Newtonian fluids have diverse applications in geoscience, petroleum industry, atmospheric sciences, oceanography, aeromechanics etc. Principle of fluid movement, heat and mass transmission via porous media plays an important role in different fields. Various properties of non-Newtonian fluids make their fundamental equations nonlinear and non-uniform. Several models have been developed to characterize attributes of non-Newtonian fluids. One of them is the Casson model. Casson [2] introduced first Casson fluid model to characterize flow of pigment oil suspensions of printing ink type and until today many investigations regarding Casson fluid have been conducted. Casson fluid is shear thinning fluid. At zero shear rate it has infinite viscosity and zero viscosity at infinite shear rate, i.e. it performs as solid if a shear stress less than yield stress is enforced to fluid and it starts to flow when shear stress is more than yield stress. Tomato sauce, jelly, chocolate, soup, honey, human blood etc. are considered as Casson fluid. At a very high shear stress Casson fluid reduced to Newtonian fluid.

Currently heat and mass transfer through porous media is centre of comprehensive research because in laminar boundary layer flow, heat-mass and momentum transfer over stretching sheet have many applications for example in increase effectiveness of paints and lubrication, in production of fiber-glass and glass blowing, in paper making industry, plastic shaping, crystallization, extrusion rubber sheets, aerodynamics etc. Mabood et al. [4] studied melting heat transfer impact on MHD Casson fluid flow through porous media. Reddy et al. [7] investigated MHD mass and heat transfer characteristic of Casson fluid over exponentially permeable stretching surface with viscous dissipation, thermal radiation and chemical reaction. Raju et al. [5] studied melting heat transfer effect on MHD Casson fluid flow through porous media with radiation in presence of first order chemical reaction. Krishnamurthy et al. [3] analyzed impact of melting heat transfer and velocity slip boundary layer flow with thermal radiation and chemical reaction on MHD nanofluid past a nonlinear stretching sheet. Yacoob et al. [8] examine stagnation-point boundary layer flow of micropolar fluid past a linearly shrinking/stretching sheet. Bachok et al. [1] investigate time independent two-dimensional flow and heat transfer to melting shrinking/stretching sheet. Lorenzini et al. [6] investigate effect of melting heat transfer in MHD Casson fluid through moving surface in porous media with radiation.

Aim of this study is to analyze impact of melting on MHD heat and mass transfer of Casson fluid flow over a stretching sheet in porous media in presence of thermal radiation and viscous dissipation.

2 Mathematical Formulation

In present study two-dimensional time independent stagnation point flow of Casson fluid past a linear stretching sheet in porous media is considered. Permeability of porous media is K_p. Sheet is melting at constant rate into warm liquid of same material, as demonstrated in figure 2.1. Transverse magnetic field B_0 is applied uniformly to fluid. Let velocity of fluid is $u_e(x) = ax$ and stretching sheet velocity is $u_w(x) = cx$, where a and c are positive constant and x coordinate considered along the stretching sheet. Let T_m represent melting temperature and T_∞ represent free stream temperature of the fluid, where $T_\infty > T_m$.

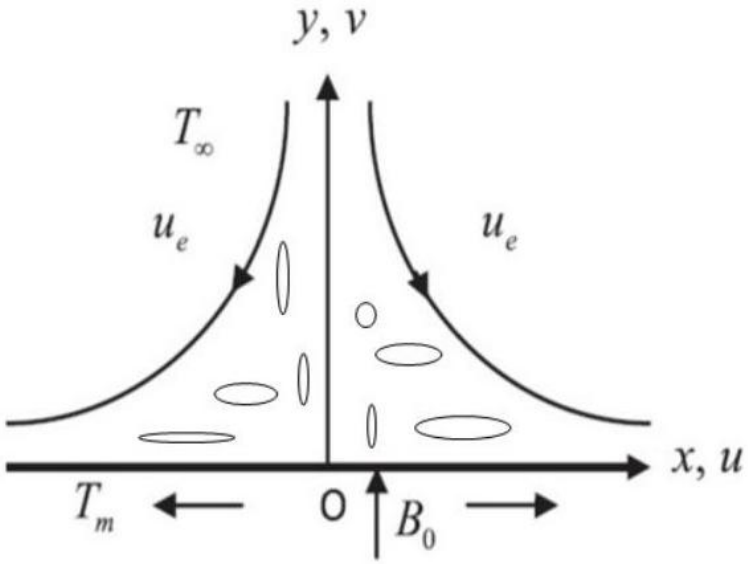

***Figure* 2.1:** Sketch of physical model

$$\tau_{ij} = \begin{cases} \left(\mu_B + (2\pi)^{\frac{1}{2}} P_y\right) 2e_{ij} & \pi > \pi_c \\ \left(\mu_B + (2\pi_c)^{\frac{1}{2}} P_y\right) 2e_{ij} & \pi < \pi_c \end{cases} \tag{2.1}$$

where μ_B represent plastic dynamic viscosity, $\pi = e_{ij}e_{ij}$ and $(i,j)^{th}$ element of deformation rate is e_{ij}, π represent rate of deformation, π_c is critical value of Casson fluid model, yield stress of fluid is P_y. Considering above postulation the governing equations of present flow are given below:

$$\frac{\partial u}{\partial x} + \frac{\partial v}{\partial y} = 0 \tag{2.2}$$

$$u\frac{\partial u}{\partial x} + v\frac{\partial u}{\partial y} = u_e\frac{du_e}{dx} + v\left(1 + \frac{1}{\beta}\right)\frac{\partial^2 u}{\partial y^2} - \frac{\sigma B_0^2}{\rho}(u - u_e) - \frac{v}{K_p}(u - u_e) \tag{2.3}$$

$$\rho c_p\left(u\frac{\partial T}{\partial x} + v\frac{\partial T}{\partial y}\right) = \kappa\frac{\partial^2 T}{\partial y^2} + \mu\left(1 + \frac{1}{\beta}\right)\left(\frac{\partial u}{\partial y}\right)^2 - \frac{\partial q_r}{\partial y}, \tag{2.4}$$

$$u\frac{\partial c}{\partial x} + v\frac{\partial c}{\partial y} = D^*\frac{\partial^2 c}{\partial y^2}. \tag{2.5}$$

Boundary conditions are:

$$u = u_w(x) = cx, \quad T = T_m, \quad C = C_m \quad \text{at} \quad y = 0, \tag{2.6}$$

$$u \to U_e(x) = ax, \quad T \to T_\infty, \quad C \to C_\infty \quad \text{as} \quad y \to \infty. \tag{2.7}$$

and

$$k\left(\frac{\partial T}{\partial y}\right) = \left[\rho c_s\left(T_m - T_0\right) + \rho\lambda\right] v(x,0). \tag{2.8}$$

Here β is Casson fluid parameter, v is kinematic viscosity, μ is factor of viscosity, K_p represent permeability of porous media, κ is thermal conductivity, σ is fluid electrical conductivity, at constant pressure specific heat is C_p, ρ is the density of fluid, radiative heat flux is q_r, D^* is molecular diffusivity, latent heat of fluid is λ.

Using Roseland's approximation for radiation, we obtain $q_r = -\left(\frac{4}{3}\frac{\sigma^*}{k_1}\right)\frac{\partial T^4}{\partial y}$, where σ^* represents Stefan-Boltzmann constant, k_1 represents mean absorption factor. By using Taylor series about the free stream temperature, we have

$$T^4 = 4TT_\infty^3 - 3{T_\infty}^4. \tag{2.9}$$

Now eqn. (2.4) converts to

$$\rho c_p\left(u\frac{\partial T}{\partial x} + v\frac{\partial T}{\partial y}\right) = \kappa\frac{\partial^2 T}{\partial y^2} + \mu\left(1+\frac{1}{\beta}\right)\left(\frac{\partial u}{\partial y}\right)^2 + \frac{16\sigma^* T_\infty^3}{3k_1\rho c_p}\frac{\partial^2 T}{\partial y^2}. \tag{2.10}$$

3 Problem Solution

Introducing similarity transformation and dimensionless parameters

$$\Psi = x(av)^{\frac{1}{2}}f(\eta), \quad \eta = \left(\frac{a}{v}\right)^{\frac{1}{2}}y, \quad \theta(\eta) = \frac{T-T_m}{T_\infty - T_m}, \quad \phi(\eta) = \frac{C-C_m}{C_\infty - C_m}. \tag{3.1}$$

where Ψ is stream function interpreted as $u = \frac{\partial \Psi}{\partial v}$ and $v = -\frac{\partial \Psi}{\partial x}$.

Using equation 2.10 into equations $2.2 - 2.5$), we get

$$\left(1+\frac{1}{\beta}\right)f''' - f'^2 + ff'' - (M+K_1)(f'-1) + 1 = 0, \tag{3.2}$$

$$(1+R)\theta'' + \Pr Ec\left(1+\frac{1}{\beta}\right)f''^2 + \Pr f\theta' = 0, \tag{3.3}$$

$$\phi'' + Scf\phi' = 0. \tag{3.4}$$

Equation (2.6) and (2.7) reduce to

$$f(0) = -\frac{Me}{Pr}\theta'(0), \quad f'(0) = \varepsilon, \quad \theta(0) = 0, \quad \phi(0) = 0, \tag{3.5}$$

$$f'(\infty) = 1, \quad \theta(\infty) = 1, \quad \phi(\infty) = 1, \tag{3.6}$$

where $\beta = \frac{\mu_B(2\pi_c)^{1/2}}{P_y}$ is Casson fluid parameter, magnetic parameter $M = \frac{\sigma B_0^2}{\rho a}, K_1 = \frac{v}{K_p a}$ permeability parameter, radiation parameter $R = \frac{16\sigma^* T_\infty^3}{3k^*\kappa}, \varepsilon = \frac{c}{a}$ stretching parameter, $\Pr = \frac{\rho c_p v}{\kappa}$ Prandtl number, combination of stefan numbers $\frac{c_s(T_m - T_0)}{\lambda}$ and $\frac{c_p(T_\infty - Tm)}{\lambda}$ respectively for solid and liquids phases is melting parameter $Me = \frac{c_p(T_\infty - T_m)}{\lambda + c_s(T_m - T_0)}$.

The physical parameters of attention are skin friction factor C_f, Nusselt number Nu_x and Sherwood number Sh_x are described as

$$C_f = \frac{\tau_W}{\rho U_e^2}, \tag{3.7}$$

$$Nu_x = \frac{xq_W}{\kappa(T_\infty - T_m)}, \tag{3.8}$$

$$Sh_x = \frac{xL_W}{D^*(C_\infty - C_m)}, \tag{3.9}$$

where τ_W represents surface shear stress, q_W denote surface heat flux and mass flux L_W are described as

$$\tau_W = \left(1+\frac{1}{\beta}\right)\left(\frac{\partial u}{\partial y}\right)_{y=0}, \tag{3.10}$$

$$q_W = -\kappa\left(\frac{\partial T}{\partial y}\right)_{y=0} + q_r, \tag{3.11}$$

$$L_W = -D^*\left(\frac{\partial C}{\partial y}\right)_{y=0}. \tag{3.12}$$

From equations (3.12) to 3.15 with applications of similarity transformations, we get

$$C_f = \left(1 + \frac{1}{\beta}\right) Re_x^{-\frac{1}{2}} f''(0), \tag{3.13}$$

$$Nu_x = -(1+R) Re_x^{\frac{1}{2}} \theta'(0), \tag{3.14}$$

$$Sh_x = -\phi'(0) Re_x^{\frac{1}{2}}, \tag{3.15}$$

where $Re_x = \frac{u_e x}{v}$ represents Reynolds number.

It is remarkable observation that if we put $M = K_1 = R = Ec = Sc = 0$ and $\beta \to \infty$ in equations (3.1) to (3.3), our problem converts into model taken by Mabood et al. [4].

4 Numerical Solution

Equations (3.2) to (3.4) are solved numerically with boundary conditions (3.5) and (3.6) by applying the shooting method together with $RK4$ scheme. For calculations we utilize MATLAB computer programming. Appropriate estimates of f'', θ' and ϕ' at $\eta = 0$ are taken with shooting method to obtain boundary conditions at $\eta \to \infty$ which all are one. We assume $\Delta\eta = 0.01$ and value for $\eta_{\max} = 5$.

In Tables 4.1, 4.2 and 4.3 validation of present method is established by comparing with results of Mabood et al. [4]

***Table* 4.1:** For varying values of ε and Me comparison of numeric values of $f''(0)$ and $\theta'(0)$, when $M = K_1 = R = Ec = Sc = 0, \Pr = 1$, and $\beta \to \infty$.

Parameters		Mabood et al. [4]		Present outcomes	
ε	Me	$f''(0)$	$-\theta'(0)$	$f''(0)$	$-\theta'(0)$
0.0	0	1.232588	-0.570465	1.232588	-0.570465
	1	1.037003	-0.361961	1.037003	-0.361961
0.5	0	0.713295	-0.692064	0.713295	-0.692064
	1	0.599090	-0.438971	0.599090	-0.438971
2.0	0	-1.887307	-0.979271	-1.887307	-0.979271
	1	-1.580484	-0.621187	-1.580484	-0.621187
5.0	0	-10.264749	-1.396355	-10.264749	-1.396355
	1	-8.5746752	-0.886425	-8.5746752	-0.886425
6.0	0	-13.774813	-1.511165	-13.774813	-1.511165
	1	-11.501531	-0.959514	-11.501531	-0.959514

***Table* 4.2:** For varying values of ε and Me comparison of numeric values of $f''(0)$, when $\Pr = 1$, $M = K_1 = R = Ec = Sc = 0$ and $\beta \to \infty$.

ε	Mabood et al. [4]			Present outcomes		
	$Me = 0$	$Me = 1$	$Me = 2$	$Me = 0$	$Me = 1$	$Me = 2$
0.0	1.232588	1.037003	0.946851	1.232588	1.037003	0.956851
0.1	1.146561	0.964252	0.880442	1.146561	0.964252	0.880442
0.5	0.713295	0.599089	0.547021	0.713295	0.599089	0.547021
1.0	0	0	0	0	0	0
2.0	-1.887307	-1.580484	-1.442747	-1.887307	-1.580484	-1.442747

***Table* 4.3:** For varying values of Pr and Me comparison of numeric values of $\theta'(0)$, when $M = K_1 = R = Ec = Sc = 0$ and $\beta \to \infty$.

Parameters		Mabood et al. [4]	Present outcomes
Pr	Me	$-\theta'(0)$	$-\theta'(0)$
1	0	-0.7978846	-0.7978846
	1	-0.5060545	-0.5060545
	2	-0.3826383	-0.3826383
7	0	-2.1110042	-2.1110042
	1	-1.3388943	-1.3388943
	2	-1.0123657	-1.0123657

5 Discussion of the Results

For computation default values are taken $\varepsilon = 0.5$ or $1.5, M = 0.5, K_1 = 0.2, \Pr = 25, R = 1, \beta = 1$, $Me = 1, Ec = 0.2, Sc = 1$.

Fig. 5.1 depicts impact of Magnetic parameter M on velocity, for $\varepsilon = 1.3$ velocity decreases with increasing values of M, this is because of Lorentz force which is retarded force for velocity. Effect is opposite for $\varepsilon = 0.3$. Influence of permeability parameter is illustrated in Fig. 5.2. It is concluded that with increasing values of K_1 velocity profile decrease because with increasing values of K_1 permeability decrease. Inverse effect found for $\varepsilon = 0.3$. From Fig. 5.3 fluid velocity is a decreasing function of Casson fluid parameter β because viscosity increased with increment in values of β and reverse results exist for $\varepsilon = 0.3$. Fig. 5.4 shows influence of β on temperature profile, here we conclude that fluid temperature decreases with increasing values of β due to the fact that increment in β signifies a reduction in yield stress. From Fig. 5.5 we observed that temperature increase with increment in values of Pr, according to definition of Prandtl number large values of Pr has lower thermal diffusivity. Because of the melting parameter, thickness of thermal boundary layer increases with increasing values of Pr. From Fig. 5.6 we observed that with increasing values of radiation parameter R temperature decrease. Fig. 5.7 depicts effect of melting parameter on temperature. Temperature profile decrease with increasing melting parameter because plunges of cold sheet in hot fluid, this starts to melt due to this temperature decreases. Fig. 5.8 shows the effect of Eckert number Ec on temperature profile, temperature increase due to viscous dissipation. Effect of Schmidt number shows in Fig. 5.9 which is analogous to effect of Prandtl number. Fig. 5.10 depicts impact of melting parameter Me on concentration. Concentration profile decrease with increasing values of Me.

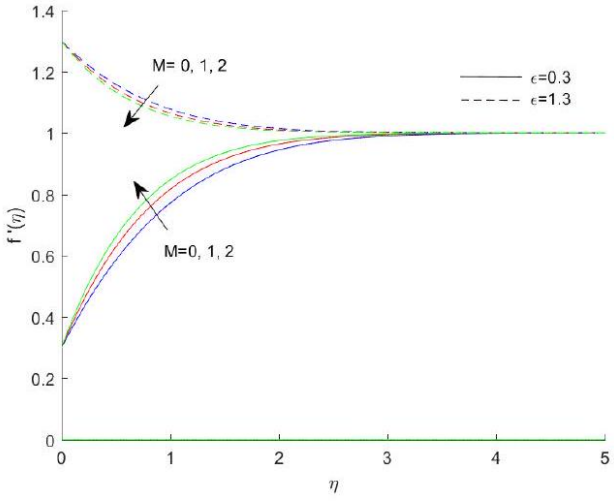

***Figure* 5.1:** Distribution of velocity for variations in M

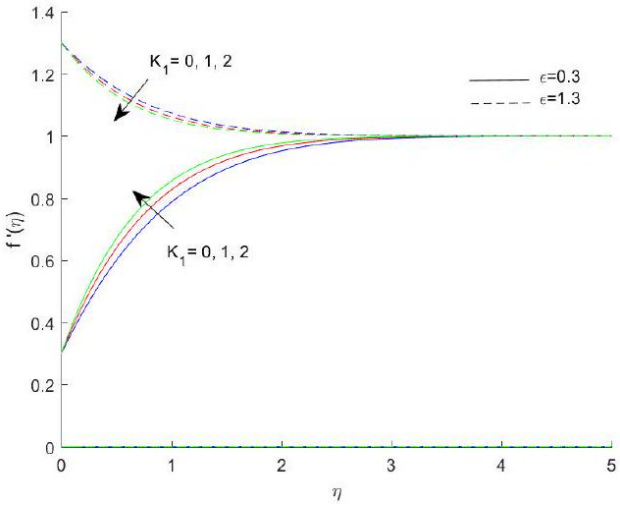

***Figure* 5.2:** Distribution of velocity for variations in K_1

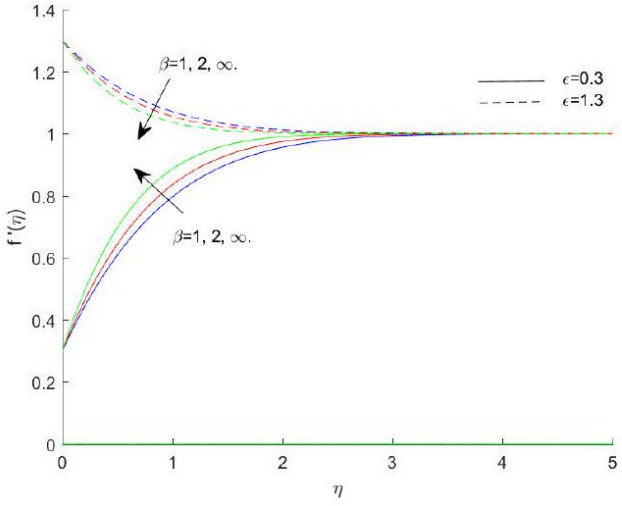

***Figure* 5.3:** Distribution of velocity for variations in β

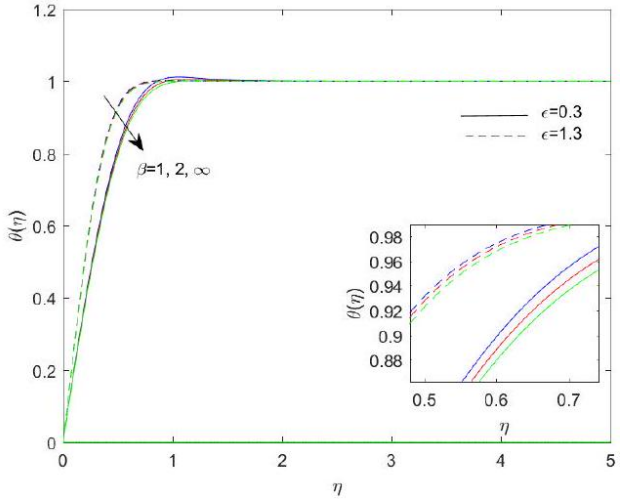

***Figure* 5.4:** Distribution of temperature for variations in β

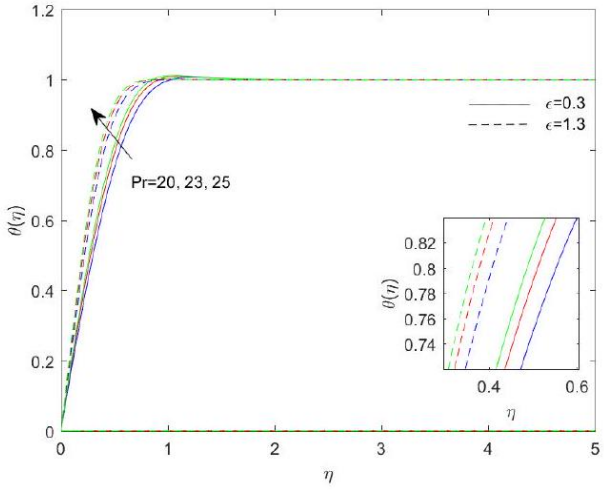

***Figure* 5.5:** Distribution of temperature for variations in Pr

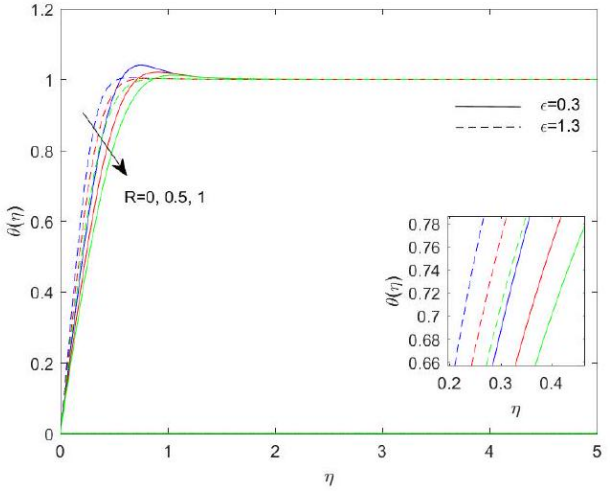

***Figure* 5.6:** Distribution of temperature for variations in R

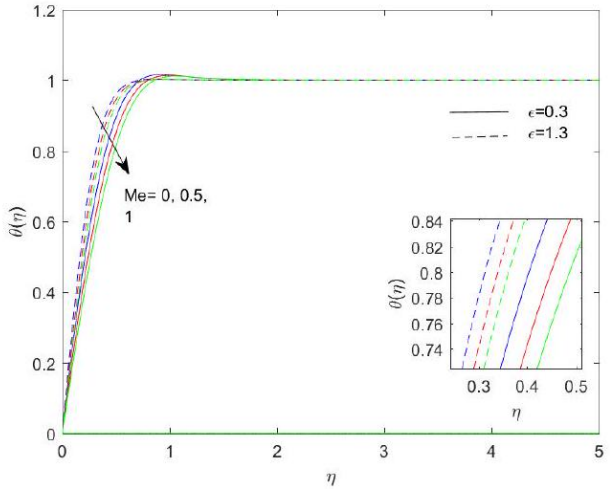

***Figure* 5.7:** Distribution of temperature for variations in Me

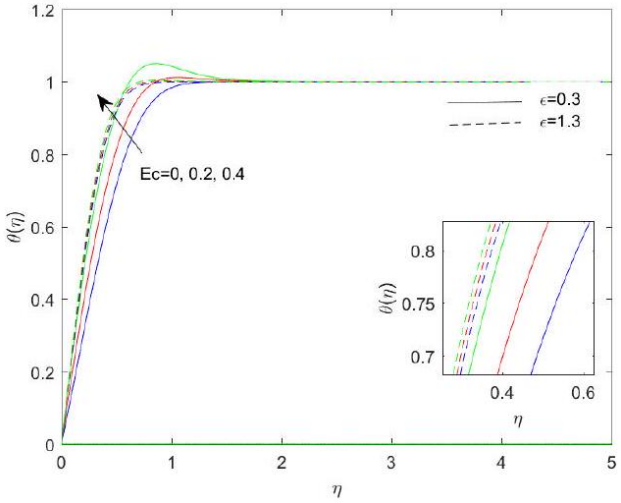

***Figure* 5.8:** Distribution of temperature for variations in Ec

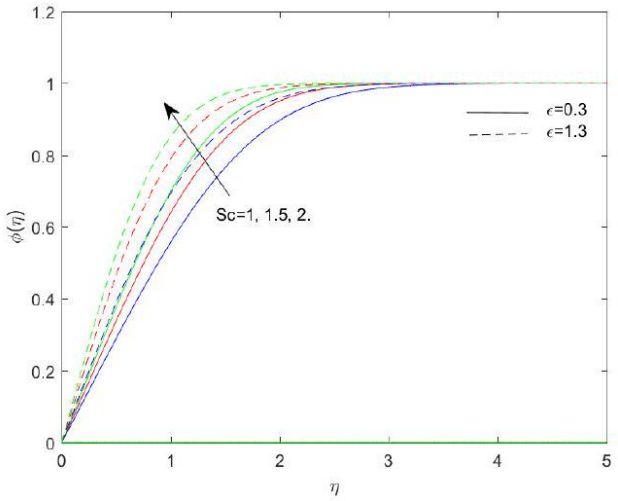

***Figure* 5.9:** Distribution of concentration for variations in Sc

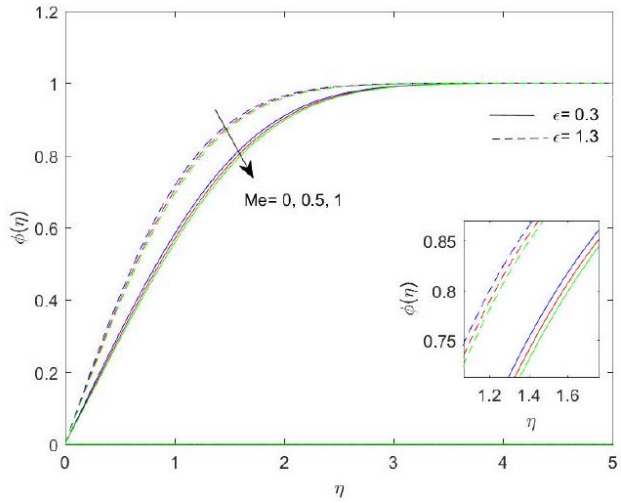

***Figure* 5.10:** Distribution of concentration for variations in Me

***Table* 5.1:** For variations in values of $\varepsilon, M, K_1, Pr, R, \beta, Me, Ec$ and Sc, Values of $f''(0), \theta'(0)$ and $\phi'(0)$.

ε	M	K_1	Pr	R	β	Me	Ec	Sc	$f''(0)$	$\theta'(0)$	$\phi'(0)$
0.3	0								0.689560	1.962200	0.571600
	1								0.844058	2.140100	0.581800
	2								0.974919	2.294100	0.588610
1.3	0								-0.362260	2.536900	0.801900
	1								-0.418174	2.553700	0.797700
	2								-0.467735	2.569500	0.794210
0.3		0							0.739190	2.018800	0.575110
		1							0.885303	2.188400	0.584100
		2							1.010939	2.337000	0.590250
1.3		0							-0.379850	2.542000	0.800530
		1							-0.433612	2.558400	0.796560
		2							-0.481646	2.574100	0.793300
0.3			20						0.768913	1.819100	0.572000
			23						0.769968	1.963200	0.575340
			25						0.770562	2.054900	0.577220
1.3			20						-0.390260	2.265200	0.792670
			23						-0.390836	2.436900	0.797180
			25						-0.391160	2.545400	0.799670
0.3				0					0.767515	2.459900	0.567530
				0.5					0.769195	2.236400	0.572900
				1					0.770562	2.054900	0.577220
1.3				0					-0.389714	3.004400	0.788400
				0.5					-0.390500	2.754800	0.794500
				1					-0.391160	2.545400	0.799670
0.3					1				0.770562	2.054900	0.577220
					2				0.887272	2.028200	0.589700
					∞				1.081560	1.997400	0.606880
1.3					1				-0.391160	2.545400	0.799670
					2				-0.450310	2.529000	0.795800
					∞				-0.548753	2.505400	0.790200
0.3						0			0.786170	2.727100	0.627570
						0.5			0.777282	2.332700	0.598750
						1			0.770562	2.054900	0.577220
1.3						0			-0.399250	3.329300	0.863780
						0.5			-0.394662	2.874700	0.827300
						1			-0.391160	2.545400	0.799670
0.3							0		0.775080	1.456900	0.591700
							0.2		0.770562	2.054900	0.577220
							0.4		0.766326	2.618400	0.563800
1.3							0		-0.391540	2.424300	0.802700
							0.2		-0.391160	2.545400	0.799670
							0.4		-0.390780	2.665400	0.796700
0.3								1	0.770562	2.054900	0.577220
								1.5	0.770562	2.054900	0.673100
								2	0.770562	2.054900	0.747800
1.3								1	-0.391160	2.545400	0.799670
								1.5	-0.391160	2.545400	0.969400
								2	-0.391160	2.545400	1.108200

6 Conclusions

In this paper a theoretical analysis of impact of melting on MHD heat and mass transfer of Casson fluid flow over a stretching sheet in porous media in the presence of thermal radiation and viscous dissipation have been done. We have acquired following results:

6.1 An increase in Magnetic parameter M, Casson fluid parameter β and Permeability parameter K_1 causes decreases in velocity profile.

6.2 Temperature profile decrease with increasing Casson fluid parameter, Melting parameter, Radiation parameter and reverse effect for Prandtl number and Eckert number.

6.3 Concentration profile increase for increasing Schmidt number and decrease for Melting parameter.

6.4 Increment in values of Magnetic parameter and Permeability parameter skin friction coefficient increase.

6.5 Local Nusselt number decrease with increasing values of radiation and melting parameter.

Acknowledgement. The authors are grateful to the Editor and Reviewer for the suggestions which led to the paper in the present form.

References

[1] N. Bachok, A. Ishak and I. Pop, Melting heat transfer in boundary layer stagnation-point flow towards a stretching/shrinking sheet, *Physics Letters A,* **374** (2010), 4075-4079.

[2] N. Casson, *A flow equation for pigment oil-suspensions of the printing ink type, Rheology of Disperse Systems,* C.C. Mill [Ed.], Pergamon Press London, 1959, 84-104.

[3] M.R. Krishnamurthy, B.J. Gireesha, B.C. Prasannakumara and R. S. R. Gorla, Thermal radiation and chemical reaction effects on boundary layer slip flow and melting heat transfer of nanofluid induced by a nonlinear stretching sheet, *Nonlinear Engineering, De Gruyter,* **5**(3) (2016), 147-159.

[4] F. Mabood and K. Das, Outlining the impact of melting on MHD Casson fluid flow past a stretching sheet in a porous medium with radiation, *Heliyon*, **5** (2019), 2405-8440.

[5] R. Mohana Ramana, J. Girish Kumar and K. Venkateswara Raju, Melting and radiation effects on MHD heat and mass transfer of Casson fluid flow past a permeable stretching sheet in the presence of chemical reaction, *AIP Conference Proceedings 2246,* **020021** (2020), 1-15.

[6] F. Mabood, R. G. Abdel Rahman and G. Lorenzini, Effect of melting heat transfer and thermal radiation on Casson fluid flow in porous medium over moving surface with magnetohydrodynamics, *Journal of Engineering Thermophysics,* **25**(4) (2016), 536-547.

[7] C.S.K. Raju, N. Sandeep, V. Sugunamma, M. Jayachandra and J.V. Ramana Reddy, Heat and mass transfer in magneto hydrodynamic Casson fluid over an exponentially permeable stretching surface, Engineering Science and Technology, *An International Journal,* **19** (2016), 45-52.

[8] N. A. Yacob, A. Ishak and I. Pop, Melting heat transfer in boundary layer stagnationpoint flow towards a stretching/shrinking sheet in a micropolar fluid, *Computers & Fluids,* **47** (2011), 16-21.